Secondary structure of human apolipoprotein A-I(1–186) in lipid-mimetic solution

Mark Okon[a], Philippe G. Frank[b], Yves L. Marcel[b], Robert J. Cushley[a],*

[a]*Department of Molecular Biology and Biochemistry, Simon Fraser University, 8888 University Drive, Burnaby, B.C., Canada V5A 1S6*
[b]*Lipoproteins and Atherosclerosis Research Group, University of Ottawa Heart Institute, Ottawa, Ont., Canada K1Y 4E9*

Abstract The solution structure of an apoA-I deletion mutant, apoA-I(1–186) was determined by the chemical shift index (CSI) method and the torsion angle likelihood obtained from shift and sequence similarity (TALOS) method, using heteronuclear multidimensional NMR spectra of [u-^{13}C, u-^{15}N, u-50% ^{2}H]apoA-I(1–186) in the presence of sodium dodecyl sulfate (SDS). The backbone resonances were assigned from a combination of triple-resonance data (HNCO, HNCA, HN(CO)CA, HN(CA)CO and HN(COCA)HA), and intraresidue and sequential NOEs (three-dimensional (3D) and four-dimensional (4D) ^{13}C- and ^{15}N-edited NOESY). Analysis of the NOEs, H$^{\alpha}$, C$^{\alpha}$ and C′ chemical shifts shows that apoA-I(1–186) in lipid-mimetic solution is composed of α-helices (which include the residues 8–32, 45–64, 67–77, 83–87, 90–97, 100–140, 146–162, and 166–181), interrupted by short irregular segments. There is one relatively long, irregular and mostly flexible region (residues 33–44), that separates the N-terminal domain (residues 1–32) from the main body of protein. In addition, we report, for the first time, the structure of the N-terminal domain of apoA-I in a lipid-mimetic environment. Its structure (α-helix 8–32 and flexible linker 33–44) would suggest that this domain is structurally, and possibly functionally, separated from the other part of the molecule. © 2001 Federation of European Biochemical Societies. Published by Elsevier Science B.V. All rights reserved.

Key words: Protein structure; Apolipoprotein; NMR; Chemical shift index; TALOS; SDS

1. Introduction

Apolipoprotein A-I (apoA-I) is the principal protein component of high density lipoproteins (HDL) and is responsible for the formation of HDL particles. ApoA-I is the major activator of the enzyme LCAT, which participates in a key step in the reverse transport of cholesterol. Reverse cholester-ol transport involves diffusion of unesterified cholesterol from peripheral tissue to lipoproteins, esterification of lipoprotein cholesterol by LCAT and lipoprotein transport of esterified cholesterol to the liver for catabolism and excretion into the bile [1].

ApoA-I is hydrophobic, aggregates in aqueous solution, and has two 11 and eight 22 residue tandem repeats, which were proposed to form amphipathic helices with distinct hydrophilic and hydrophobic faces [2,3]. It is known from mutant proteins [4,5] and mutagenesis studies [6–8] that certain regions of apoA-I are responsible for lipid binding and activation of LCAT.

In the present communication we report the preparation by bacterial expression, and a multidimensional heteronuclear NMR study of [u-^{13}C; u-^{15}N; u-50% ^{2}H]apoA-I(1–186). The NMR spectra were determined in excess SDS. NMR studies of lipid-associating proteins are often conducted in the presence of SDS which serves as a model for a membrane environment [9,10]. SDS micelles are ∼5 nm in diameter, which is similar in size to the pre-β-HDL and to the smallest HDL$_3$, hence are likely to yield a conformation resembling the apoA-I structure present in HDL. In fact, SDS was shown to model the lipoprotein environment for apoA-I peptides [11–13].

From the heteronuclear NMR data we were able to assign the backbone atom (^{1}H, ^{13}C and ^{15}N) chemical shifts and to establish the solution secondary structure of apoA-I(1–186) in a lipid-mimetic environment. To our knowledge, this is the largest exchangeable apolipoprotein, whose solution lipid-bound structure has been resolved.

2. Materials and methods

2.1. Sample production and purification
The C-terminal deletion mutant, apoA-I(1–186), molecular weight 23 067, includes the N-terminal extension Met-Arg-Gly-Ser-(His)$_6$-Met [14]. It was expressed in a bacterial system described earlier [15], using Martek 9-CN media containing 98% ^{13}C and ^{15}N with 50% ^{2}H (Martek Biosciences, Columbia, MD, USA). After purification on nitriloacetic acid agarose (NTA, Qiagen), the uniformly labeled protein (7.5 mg/l media) was dialyzed against 5 mM NH$_4$HCO$_3$, and lyophilized.

2.2. Circular dichroic measurements
Circular dichroic spectroscopy was performed using a Jasco J41A spectropolarimeter, as previously described [8]. The percentage of α-helix content was calculated from the molar ellipticity at 222 nm and using a mean residue weight of 115.2 for native apoA-I and 115.5 for apoA-I(1–186).

2.3. NMR spectroscopy
A 1 mM solution of [u-^{13}C; u-^{15}N; u-50% ^{2}H]apoA-I(1–186) in

95% H_2O:5% D_2O, 3 mM EDTA, pH 6.4, was prepared containing SDS–d_{25}. The protein:SDS ratio was 1:140 mol/mol. NMR spectra were recorded at 39°C on a Bruker AMX-600 spectrometer operating at 600.13 MHz (^{1}H) and equipped with a Z-gradient triple-resonance probe.

A two-dimensional (2D) ^{1}H/^{15}N HSQC spectrum [16] was acquired with 256×256 complex points and spectral widths of 5.667 (^{1}H) and 31.145 (^{15}N) ppm (64 transients).

The 3D ^{15}N-edited, gradient-enhanced NOESY-HSQC [17] spectrum was recorded with a mixing time of 150 ms. Due to hardware and software restrictions, only four pulse field gradients instead of 12, and a smaller number of hard ^{15}N pulses, were used. A series of constant time (CT) triple-resonance pulse sequences, CT-HNCO, CT-HNCA and CT-HN(CO)CA [18], were used with the following modifications: (i) pulse field gradients were used to minimize the artifact content of the spectra [19] and (ii) a WATERGATE pulse sequence was used to suppress the water signal [20]. A CT-HN(CA)-CO experiment was used, which was a modification of the 3D CT-HN(CO)CA mentioned above and where an HSQC instead of an HMQC step in the C'-C$^\alpha$ magnetization transfer was inserted. Finally, a 3D HN(COCA)HA experiment was used, based on a 4D HN(CO)CAHA pulse sequence [21] without a C$^\alpha$ evolution time. WATERGATE and pulse field gradient sequences were added as well. The CBCA(CO)NH experiment [22] was made without modifications.

A 4D ^{15}N/^{13}C-edited NOESY [23] spectrum was recorded based on the 3D ^{15}N-edited gradient-enhanced NOESY-HSQC spectrum (see above). A 4D ^{15}N/^{13}C'-edited NOESY-HNCO spectrum was recorded using the 3D ^{13}C'-edited NOESY-H(N)CO pulse sequence [24] to which a ^{15}N dimension was added.

In general, the acquisition dimension was collected with a spectral width of 2.4 ppm, using 256 complex points with the carrier position at 8.0 ppm (the center of the HN region). Spectral widths in the indirectly detected ^{15}N, ^{13}C' and ^{13}C$^\alpha$ dimensions were 24.0, 12.1, and 31.14 ppm, respectively, with the carrier positions at 116.5, 177.0, and 56.0 ppm, respectively. The number of acquired complex points for 3D CT experiments were 30 for ^{15}N and 48 for ^{13}C and mirror linear prediction was used to increase the resolution in the ^{15}N dimension. For the CT-HN(COCA)HA experiment the spectral width for indirectly detected ^{1}H was 2.0 ppm, using 28 complex points with the carrier set at 4.33 ppm.

The 4D ^{15}N/^{13}C-edited NOESY was collected with spectral widths of 2.4, 24.0, 7.6, and 23.9 ppm in directly detected H^N and indirectly detected ^{15}N, ^{1}H, and ^{13}C dimensions, respectively. The numbers of acquired complex points were 256, 16, 64, and 16, respectively. The spectral widths and numbers of acquired complex points for 4D ^{15}N/^{13}C'-edited NOESY-HNCO were 2.4, 9.0, 24.0, and 8.5 ppm and 128, 64, 14, and 6 points in H^N, ^{1}H, ^{15}N, and ^{13}C' dimensions, respectively.

The numbers of transients were 8–96 for 3D and 1–2 for 4D experiments. Proton chemical shifts were referenced to internal 2,2-dimethyl-2-silapentane-5-sulfonic acid (DSS) directly, and ^{13}C and ^{15}N chemical shifts were indirectly referenced to DSS [25].

Data were processed and analyzed on an SGI O2 workstation using nmrPipe/nmrDraw [26] and NMRView3 [27]. NMRView3 was also used for sequential assignments. The chemical shift data will be available from the BioMagResBank after 09/01/2001.

2.4. Structure analysis

The secondary structure was determined from the ^{1}H, ^{13}C and ^{15}N chemical shift values using CSI [25,28–30] and the TALOS program [31]. Secondary chemical shifts used as input for CSI were calculated by subtracting the measured chemical shifts of apoA-I(1–186) in SDS–d_{25} complexes from the corresponding random coil values [32]. A combination of four kinds (^{1}H$^\alpha$, ^{13}C$^\alpha$, ^{13}C' and ^{15}N) of chemical shifts was used for TALOS [31] prediction of phi and psi backbone torsion angles. TALOS uses shift data for three consecutive residues, the 'triplet', and compares it with similar triplets in a database. The 10 best matches to a given triplet were tested for consistency of phi and psi angles and their averages and standard deviations were used for predicting apoA-I(1–186) structure. The TALOS database contains 20 proteins with known high resolution crystal structures (3032 triplets). Although Fig. 3 represents the exact values of predicted TALOS angles, TALOS structure predictions were analyzed exclusively in a CSI-like manner in accordance with the following relationships:

TALOS prediction	CSI analog
Good prediction for α-helix conformation	+1
No definite prediction	0
Good prediction for β-(extended) conformation	−1

Then, CSI and TALOS predictions were analyzed in common using CSI rules. The resulting apoA-I(1–186) structure (depicted in Figs. 3 and 4) is the result of consensus between CSI and TALOS.

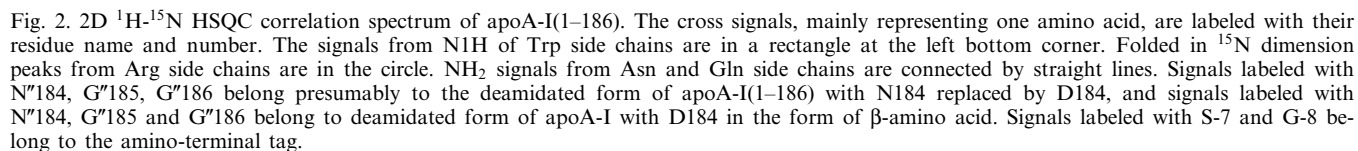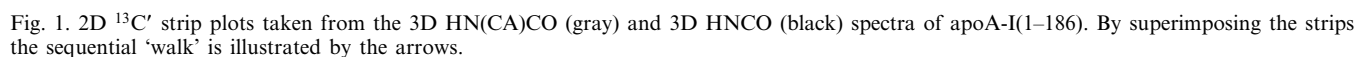### 2.5. ApoA-I(1–186) backbone flexibility

Relative flexibility along the backbone chain was estimated by comparing the signal intensities in the 3D HNCO spectrum. The line intensity in this type of spectrum is a complex function of defocusing and refocusing delays in the pulse sequence, the T_2 values (or ^{1}H^N, ^{15}N and ^{13}C' line widths) and the spin–spin coupling constants $^1J_{NH}$ and $^1J_{NC'}$. All of these parameters, except T_2 values, are essentially the same for each amino acid in a protein, so the difference in line intensities will be, to first approximation, a function of only the corresponding T_2 values. In other words, the 3D HNCO pulse sequence works like a T_2 filter, and is the main reason it is impossible to get 3D spectra for large proteins with short T_2 values. In turn, the T_2 values are functions of magnetic interactions between nuclei (that are, again, mainly the same for backbone H^N, N and C' of each residue), and of flexibility of the amino acid residue. Thus, the difference in line intensities in a 3D HNCO spectrum is mainly related to the difference in flexibility along the protein backbone chain, with greater line intensity corresponding to greater flexibility.

3. Results

ApoA-I(1–186), which lacks the C-terminal fragment, residues 187–243 in the native protein, is secreted as a normally folded protein. CD analyses of the lipid-free protein indicate a 45.5% α-helix content compared to 49% for native apoA-I. Like wild-type apoA-I, it binds phospholipids in the presence of cholate and can form discoidal lipoproteins with two apoA-I per particle that elicit normal rates of diffusional cellular cholesterol efflux [15]. Deletion of residues 187–243 removes a high affinity lipid binding domain [33] and, as expected, apoA-I(1–186) displays a reduced DMPC clearance and reduced ability to mobilize cellular lipids [15].

3.1. Strategy for assignment of apoA-I(1–186) NMR spectra

The backbone resonances were assigned from a combination of triple-resonance constant time experiments (HNCO, HNCA, HN(CO)CA and HN(CA)CO), and intraresidual and sequential NOEs (3D ^{15}N-edited NOESY). Sequential assignments of backbone H^N, ^{15}N^H, ^{13}C$^\alpha$ and ^{13}C' signals were obtained from correlation of sequential and intraresidual scalar connectivities observed in the series of 3D experiments. Intraresidual C$^\alpha$(i)-N(i)-H(i) and sequential C$^\alpha$(i−1)-N(i)-H(i) scalar connectivities were taken from HNCA and HN(CO)CA spectra, respectively. Some C$^\alpha$(i−1)-N(i)-H(i) scalar connectivities were observed in the HNCANH spectrum. Intraresidual C'(i)-N(i)-H(i) and sequential C'(i−1)-N(i)-H(i) scalar connectivities were taken from HN(CA)CO and HNCO spectra, respectively. The pattern of 'walking strategy' is illustrated by the superposition of HNCO and HN(CA)CO spectra (Fig. 1). In some cases this kind of double scalar correlation between adjacent amino acid residues was not sufficient for unambiguous assignment and additional NOE information concerning sequential d$_{NN}$ connectivities was used from the ^{15}N-edited NOESY-HSQC spectrum. The H$^\alpha$ chemical shifts were extracted from the HN(COCA)HA spectrum. The types of amino acids were determined from the CBCA(CO)NH spectrum, when it was possible. Otherwise, they were determined from ^{15}N-edited NOESY-HSQC, to-

Fig. 1. 2D $^{13}C'$ strip plots taken from the 3D HN(CA)CO (gray) and 3D HNCO (black) spectra of apoA-I(1–186). By superimposing the strips the sequential 'walk' is illustrated by the arrows.

Fig. 2. 2D ^1H-^{15}N HSQC correlation spectrum of apoA-I(1–186). The cross signals, mainly representing one amino acid, are labeled with their residue name and number. The signals from N1H of Trp side chains are in a rectangle at the left bottom corner. Folded in ^{15}N dimension peaks from Arg side chains are in the circle. NH$_2$ signals from Asn and Gln side chains are connected by straight lines. Signals labeled with N″184, G″185, G″186 belong presumably to the deamidated form of apoA-I(1–186) with N184 replaced by D184, and signals labeled with N″184, G″185 and G″186 belong to deamidated form of apoA-I with D184 in the form of β-amino acid. Signals labeled with S-7 and G-8 belong to the amino-terminal tag.

gether with the unique combination of ^{15}N, ^{13}C$^\alpha$ and ^{13}C$'$ signal chemical shifts.

Because of specific sequence Pro3-Pro4, i.e. with no H^N proton at Pro4, the signals from Pro3, as well as Glu110 and Pro121, were not found. The HN signals from the first Met and Arg as well as from five His residues in the 11 residue 'leader' were not found probably due to fast exchange with solvent, thus implying an absence of regular structure for this region. Consistent with this finding, it was shown that this amino-terminal tag of six histidines added to native apoA-I does not change the physicochemical properties of the protein or its ability to interact with phospholipids and to promote cholesterol esterification and cellular cholesterol efflux [14].

3.2. Characteristics of apoA-I(1–186) heteronuclear 2D NMR spectra in SDS solution

The 2D ^{1}H/^{15}N HSQC spectrum of apoA-I(1–186) is shown in Fig. 2. A very small dispersion of H^N chemical shifts, only 1.2 ppm, is apparent. This small dispersion, as well as broad (20–30 Hz) proton line widths, lead to strong signal overlap in the HSQC spectrum. Only 55–60 signals (about 30%), mainly from Ala, Thr, Ser and Gly residues, are well resolved in the HSQC spectrum. The strong overlapping signals made it difficult to assign shifts from HSQC-based 3D spectra like NO-ESY, and to obtain suitable relaxation measurements to describe intramolecular dynamics. Only 3D ^{1}H/^{13}C/^{15}N experiments give well resolved apoA-I(1–186) spectra. Another feature of the apoA-I(1–186) 2D HSQC and 3D spectra – the wide range of signal intensities – will be described in Section 3.4.

3.3. Secondary structure of apoA-I(1–186) in SDS solution

The secondary structure of apoA-I(1–186) is shown in Fig. 3. Residues 1–6 are 'unordered'. That is, they are not truly random coil because, while CSI does not predict any definite structure, the Φ, Ψ plot (Fig. 3) shows phi and psi matches for some contribution from β-(extended) structures accompanied by strong RMS deviations (Fig. 4) in the TALOS prediction. Residues 8–32 form a well-defined helix. The helix appears distorted at the Gly26 position, which may be the result of
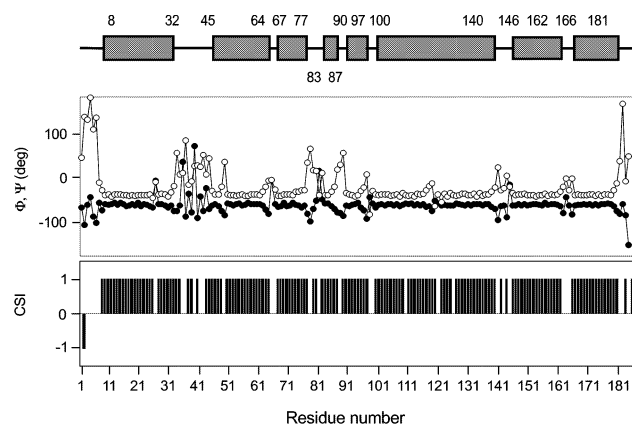

Fig. 3. Summary of structural information obtained from NMR spectra. From bottom to top: consensus of H$^\alpha$, ^{13}C$^\alpha$ and C$'$ CSI values; phi (filled circles) and psi (open circles) angle values predicted by TALOS; apoA-I(1–186) solution secondary structure (α-helices are depicted by rectangles and irregular regions by lines). The average backbone torsion angles among all well-defined α-helices (RMSD ≤ 8 degrees) are: $\Phi_{aver} = -63.2 \pm 1.8$ and $\Psi_{aver} = -42.2 \pm 1.7$ degrees.
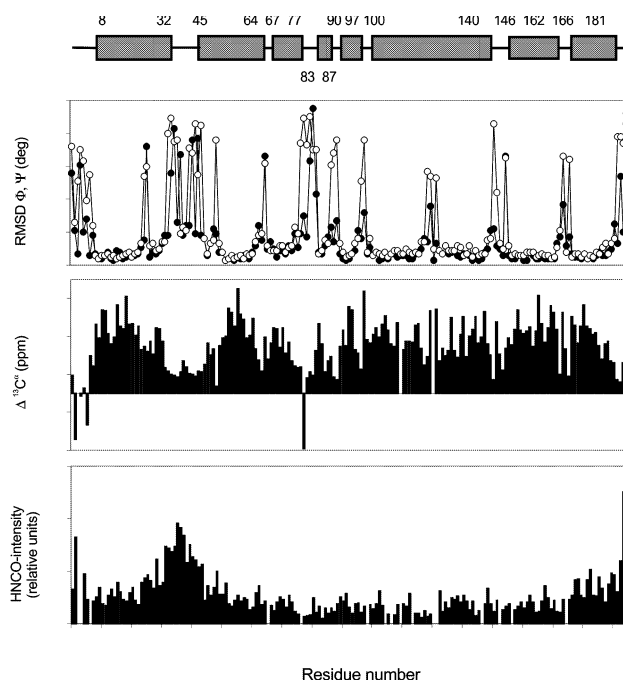

Fig. 4. Flexibility of apoA-I(1–186) in solution. From bottom to top: Line intensities in 3D HNCO spectrum; ^{13}C$^\alpha$ secondary chemical shifts; RMS deviations of phi (filled circles) and psi (open circles) values obtained by TALOS; apoA-I(1–186) solution secondary structure.

a bend. Residues 33–44 are unordered. Residues 45–64 constitute the next α-helix (the first predicted tandem helical repeat (3)). Some distortion of the helix may take place at the Asn49 position. Residues 67–77 adopt an 11-mer α-helix (exactly three turns of an ideal α-helix). However, the region 78–82 appears to be unstructured, with the helix resuming for the next five residues (83–87). Segment 88–98, predicted helical repeat 3, is the first of two predicted 11-mer helices and CSI and TALOS calculations confirm an α-helical region except the first two (Lys88 and Asp89) and last one (Glu98) residues.

Starting at Pro99 the segment 99–120, helical repeat 4, is an α-helical region (except Pro99). Segment 121–142, helical repeat 5, is a continuation of the previous α-helix except for Lys141 and Ser142. Thus, there is probably an unbroken helical segment of 41 residues in this region (Fig. 3). Segment 143–164, helical repeat 6, consists of an α-helix from 146 to 162. Segment 165–186, helical repeat 7, consists of α-helix from 166–181, according to TALOS, and we include Pro165 as a helix initiator. The rest of the protein (residues 182–186) does not appear to have a definite structure but this is no doubt due to fraying of the C-terminus. It is interesting to note that the domain of apoA-I involved in LCAT activation is helix 6 (residues 144–165) [8,34,35], although adjacent helices, mostly helix 7, partially contribute to activation [35].

Comparison of HNCA, HN(CO)CA and CBCA(CO)NH spectra of apoA-I(1–186) shows that Asn184 is mainly in the form of β-amino acid (58%), which can be a consequence of spontaneous deamidation to Asp184.

3.4. Overall flexibility of apoA-I(1–186) in lipid complexes

The salient feature of the NMR spectra of the protein is the wide range of signal intensities along the sequence. The ratios I_{max}/I_{min} from the 3D HNCO vary greater than 10-fold (Fig.

4, bottom), which undoubtedly is a consequence of different flexibility along the polypeptide chain (see Section 2). Another parameter that may be used to provide a qualitative picture of protein flexibility, is secondary chemical shifts. Flexible backbone regions exhibit secondary chemical shifts closer to random coil values [28].

It can be seen that the line intensities (Fig. 4, bottom) decay almost monotonically from the ends to the middle of the protein, except for the maxima in the region 32–44. This corresponds to decreasing backbone chain flexibility as the middle of the protein is approached from either end. For the region 32–44, the greater HNCO intensities and decreased $^{13}C^{\alpha}$ secondary shifts (Fig. 4, middle) complement each other very well. The calculated RMS deviations from TALOS predicted phi and psi angles are also increased dramatically in this region (Fig. 4, top). One immediately apparent conclusion from this comparison is that there is a very flexible region from residue 32 to 44. Flexibility of this region seems to be comparable with the flexibility of the last six C-terminal residues and it allows the helical structural domain at the N-terminus (8–32) to act independently from the majority of the apoA-I(1–186) structural element. The other helices (helical repeats 1–7) form parts of a long, continuous helical structure interrupted by 2–5 residue irregular regions, whose individual flexibility is comparable with the overall flexibility of the main chain (Fig. 4, bottom). Furthermore, the reduced secondary chemical shift values and increased RMS deviations of predicted phi and psi angles, which are typical for these regions (Fig. 4, middle and top), lead us to propose a relatively slow intrinsic mobility in the irregular interhelical regions, allowing the helical repeats to change their reciprocal orientation. This mobility would allow the protein to optimally adopt a different conformation as conditions warrant.

4. Discussion

4.1. Comparison of CSI and TALOS predictions

There were almost no discrepancies between CSI and TALOS predictions along the polypeptide chain with the exception of proline residues at the beginning of α-helices, which were assigned by TALOS to α-helix configuration, whereas strong CSI criteria ($^{13}C'$, $^{13}C_{\alpha}$ secondary shift > 4 ppm [30]) excluded the proline residues from an α-helix configuration. Some other disagreements were found at the ends of α-helices. For example, the end of helix G* (residues 33, 34) and the beginning of helical repeat 1 (residues 43, 44) were assigned by CSI to α-helix, whereas TALOS did not give any definite predictions for these residues.

4.2. Comparison with other apoA-I structures

We compared the region 142–187 in apoA-I(1–186) with the high resolution solution structure of the synthetic peptide, apoA-I(142–187) [13], under identical conditions (aqueous solution in the presence of SDS). The structures are almost identical and consist of two α-helices: 146–162 and 168–182 in the synthetic peptide and 146–162 and 166–181 in apoA-I(1–186).

The NMR-derived secondary structure of apoA-I(1–186) in lipid-mimetic solution resembles the monomer unit of the A/B dimer in the four helix bundle determined by Borhani et al. [36] from X-ray data of lipid-free tetramers of apoA-I(44–243). The exceptions are 2–5 residue irregular segments be-

tween helical repeats and an irregular unpredicted segment, residues 78–82, in helical repeat 2. However, our data do not support the presence of dimers or tetramers of apoA-I in an SDS complex. SDS–polyacrylamide gel electrophoresis of the [u-^{13}C; u-^{15}N; u-50% ^{2}H]apoA-I(1–186) showed that it is a monomer in SDS. In addition, we did not see any NMR indications of the presence of dimers or tetramers in solution like double or extremely broadened sets of peaks.

The absence of any oligomeric structure in a lipid environment may be due to the addition of residues 1–43, which, when deleted, results in an increased apoA-I oligomerization [36,37].

4.3. Irregular segments of apoA-I(1–186) between helical repeats

A characteristic of apoA-I is its lability, i.e. its ability to change conformation in order to bind to small (HDL) or large (VLDL) lipoprotein complexes, and to activate LCAT. This is not apparent from the rigid X-ray structure of lipid-free apoA-I(44–243) [36]. The X-ray structure consists of four molecules in the asymmetric unit, each molecule structure consisting 'almost entirely of a pseudocontinuous, amphipathic α-helix' [36], although the X-ray structure is not an ideal α-helix. The authors note 'bends' and 'kinks' at proline positions. Mean kink angle and its standard deviation are larger than that found in other structures and 'regions of monomer involved in crystal packing contacts are better ordered than those that are not' [36]. They also describe one mostly mobile, extended, non-helical region at the beginning of helical repeat 10 (residues 220–227).

It is quite possible that 'bends' and 'kinks' between helices found in crystal apoA-I(44–243) structure (which is additionally stabilized by 'monomer–monomer' and 'dimer–dimer' interactions) become less rigid and/or more disordered in solution (and in the complex with lipid). This should lead to an increasing number of possible local and global conformations. Our solution apoA-I(1–186) structure consisting of a number of rigid helices connected by flexible links can explain the labile properties of apoA-I.

Another result of the present apoA-I(1–186) NMR structure, which is not present in X-ray [36] or predicted [3] apoA-I structures, is an irregular segment, 78–82, in the helical repeat 2 (residues 66–87). It is interesting to note that Glu78 at the beginning of this segment is at the 13th position of the 22 residue helical repeat 2. It was found [38] that the presence of glutamic acid at the 13th position in peptide analogues of apoA-I leads to reduced lipid affinity together with an increased LCAT activating ability of the peptide. It was also shown that inclusion of a proline within the sequence of putative helix also decreases the lipid affinity of the peptide [39]. The reduced lipid affinity of the amphipathic segment may distort or destroy its helical structure, because interaction with lipid has a profound effect on the conformation of protein that interacts with it [3]. Consequently, our findings, summarized in Figs. 3 and 4, of irregular segments of 2–5 residues may result from specific protein–lipid interaction.

4.4. N-terminal domain

This is the first report of the structure of the N-terminal segment of apoA-I, residues 1–43, as a part of apoA-I(1–186). It was predicted that this region contains an amphipathic (class G*) helix comprising residues 8–33 whereas regions 1–

7 and 34–43 are disordered [3]. The amino-terminus (residues 1–33) of apoA-I is highly conserved among different apolipoprotein species and was initially thought to be a functional domain of apoA-I [40]. The estimations of lipid affinity of this domain, using model peptides, were not straightforward, changing from 'weak, if at all' [3] to 'moderate' [41]. The structure of the corresponding peptide, consisting of this domain, was random in buffer and adopted a helical conformation (52% helicity) in the presence of lipid micelles [41]. Taking into account that deletion of segment 1–43 'has no measurable effect on apoA-I lipid association' [42], this domain was arbitrarily assigned a compact globular structure in a molecular belt model for apoA-I in discoidal HDL [43]. Deletion of the domain was shown to induce oligomer formation of apoA-I [36,37], thus it may therefore be involved in the stabilization of apoA-I in its lipid-free or -poor form like in pre-β_1-HDL, and its deletion changes the conformation of lipid-free apoA-I to that of lipid-bound [42].

Our data show that the N-terminal segment of apoA-I(1–186), residues 1–44, contains an α-helical region 8–32 in the complex with SDS whereas regions 1–7 and 33–44 are disordered. That is in a good agreement with prediction [3] and gives a mean value of 76% helicity for domain 1–33. The two features of the N-terminal domain, its moderate lipid affinity [41], which is confirmed by the fact that we observe the formation of an amphipathic helical region from residues 8–32 in the presence of SDS, and the separation of this helix from the next one by an unordered linker from residue 33 to residue 44 (Figs. 3 and 4), prompt us to suggest a primary anchor role for this domain. That is, the N-terminal helix's lipid binding properties and independence would easily allow it to lift off the lipoprotein surface for binding to cell surfaces or receptors. Burgess et al. [15] had previously suggested that apoA-I binds to a second binding site on the cell surface by the N-terminal domain (residues 1–100). This domain was also shown to interact with the central domain of apoA-I, especially in small LpA-I particles [44–46], and was proposed to regulate LCAT activation [37]. The ability of the N-terminal domain to behave independently from the rest of the molecule may therefore be important for apoA-I structure and function.

References

[1] Fielding, C.J. and Fielding, P.E. (1995) J. Lipid Res. 36, 211–228.

[2] Segrest, J.P., Jackson, R.L., Morrisett, J.D. and Gotto, A.M. (1974) FEBS Lett. 38, 247–253.

[3] Segrest, J.P., Jones, M.K., De Loof, H., Brouillette, C.G., Venkatachalapathi, Y.V. and Anantharamaiah, G.M. (1992) J. Lipid Res. 33, 141–166.

[4] Deeb, S.S., Cheung, M.C., Peng, R., Wold, A.C., Stern, R., Albers, J.J. and Knopp, R.H. (1991) J. Biol. Chem. 266, 13654–13660.

[5] Rail Jr., S.C., Weisgraber, K.H., Mahley, R.W., Ogawa, Y., Fielding, C.J., Utrman, G., Haas, J., Steinmetz, A., Menzel, H.J. and Assmann, G. (1984) J. Biol. Chem. 259, 10063–10070.

[6] Sorci-Thomas, M., Kearns, M.W. and Lee, J.P. (1993) J. Biol. Chem. 268, 21403–21409.

[7] Minnich, A., Collet, X., Roghani, A., Cladaras, C., Hamilton, R.L., Feilding, C.J. and Zannis, V.I. (1992) J. Biol. Chem. 267, 16553–16560.

[8] Frank, P.G., N'Guyen, D., Franklin, V., Neville, T., Desforges, M., Rassart, E., Sparks, D.L. and Marcel, Y.L. (1998) Biochemistry 37, 13902–13909.

[9] McDonnell, P.A. and Opella, S.J. (1993) J. Magn. Reson. B 102, 120–125.

[10] Henry, G.D. and Sykes, B.D. (1994) Methods Enzymol. 239, 515–535.

[11] Buchko, G.W., Treleaven, W.D., Dunne, S.J., Tracey, A.S. and Cushley, R.J. (1996) J. Biol. Chem. 271, 3039–3045.

[12] Wang, G., Treleaven, W.D. and Cushley, R.J. (1996) Biochim. Biophys. Acta 1301, 174–184.

[13] Wang, G., Sparrow, J.T. and Cushley, R.J. (1997) Biochemistry 36, 13657–13766.

[14] Bergeron, J., Frank, P.G., Emmanuel, F., Latta, M., Zhao, Y., Sparks, D.L., Rassart, E., Denefle, P. and Marcel, Y.L. (1997) Biochim. Biophys. Acta 1344, 139–152.

[15] Burgess, J.W., Frank, P.G., Franklin, V., Liang, P., McManus, D.C., Desforges, M., Rassart, E. and Marcel, Y.L. (1999) Biochemistry 38, 14524–14533.

[16] Kay, L.E., Keifer, P. and Saarinen, T. (1992) J. Am. Chem. Soc. 114, 10663–10665.

[17] Zhang, O., Kay, L.E., Olivier, J.P. and Forman-Kay, J.D. (1994) J. Biomol. NMR 4, 845–858.

[18] Grzesiek, S. and Bax, A. (1992) J. Magn. Reson. 96, 432–440.

[19] Bax, A. and Pochapsky, S. (1992) J. Magn. Reson. 99, 638–643.

[20] Sklenar, V., Piotto, M., Leppik, R. and Saudek, V. (1993) J. Magn. Reson. Ser. A 102, 241–245.

[21] Olejniczak, E.T., Xu, R.X., Petros, A.M. and Fesik, S. (1992) J. Magn. Reson. 100, 444–450.

[22] Grzesiek, S. and Bax, A. (1992) J. Am. Chem. Soc. 114, 6291–6293.

[23] Muhandiram, D.R., Xu, G.Y. and Kay, L.E. (1993) J. Biomol. NMR 3, 463–470.

[24] Zhang, W., Smithgall, T.E. and Gmeiner, W.H. (1996) J. Magn. Reson. Ser. B 111, 305–309.

[25] Wishart, D.S. and Nip, A.M. (1998) Biochem. Cell. Biol. 76, 153–163.

[26] Delaglio, F., Grzesiek, S., Vuister, G.W., Zhu, G., Pfeifer, J. and Bax, A. (1995) J. Biomol. NMR 6, 277–293.

[27] Johnson, B.A. and Blevins, R.A. (1994) J. Biomol. NMR 4, 603–614.

[28] Wishart, D.S., Sykes, B.D. and Richards, F.M. (1991) J. Mol. Biol. 222, 311–333.

[29] Wishart, D.S., Sykes, B.D. and Richards, F.M. (1992) Biochemistry 31, 1647–1651.

[30] Wishart, D.S. and Sykes, B.D. (1994) J. Biomol. NMR 4, 171–180.

[31] Cornilescu, G., Delaglio, F. and Bax, A. (1999) J. Biol. NMR 13, 289–302.

[32] Wishart, D.S., Bigam, C.G., Holm, A., Hodges, R.S. and Sykes, B.D. (1995) J. Biomol. NMR 5, 67–81.

[33] Palgunachari, M.N., Mishra, V.K., Lund-Katz, S., Phillips, M.C., Adeyeye, S.O., Alluri, S., Anantharamaiah, G.M. and Segrest, J.P. (1996) Arterioscler. Thromb. Vasc. Biol. 16, 328–338.

[34] Sorci-Thomas, M.G., Curtiss, L., Parks, J.S., Thomas, M.J., Kearns, M.W. and Landrum, M. (1998) J. Biol. Chem. 273, 11776–11782.

[35] McManus, D.C., Frank, P.G., Franklin, V. and Marcel, Y.L. (2000) J. Biol. Chem. 275, 5043–5051.

[36] Borhani, D.W., Rogers, D.P., Engler, J.A. and Brouillette, C.G. (1997) Proc. Natl. Acad. Sci. USA 94, 12291–12296.

[37] Frank, P.G. and Marcel, Y.L. (2000) J. Lipid Res. 41, 853–872.

[38] Anantharamaiah, G.M., Venkatachalapathi, Y.V., Brouillette, C.G. and Segrest, J.P. (1990) Arteriosclerosis 10, 95–105.

[39] Pownall, H.J., Massey, J.B., Sparrow, J.T. and Gotto, A.M., Jr. (1987) in: Plasma Lipoproteins (Gotto, A.M., Jr., Ed.), pp. 95–127, Elsevier Science, Amsterdam.

[40] Anantharamaiah, G.M. (1986) Methods Enzymol. 128, 627–647.

[41] Mishra, V.K., Palgunachari, M.N., Datta, G., Phillips, M.C.,

Lund-Katz, S., Adeyeye, S.O., Segrest, J.P. and Ananthara-maiah, G.M. (1998) Biochemistry 37, 10313–10324.

[42] Rogers, D.P., Brouillette, C.G., Engler, J.A., Tendian, S.W., Roberts, L., Mishra, V.K., Anantharamaiah, G.M., Lund-Katz, S., Phillips, M.C. and Ray, M.J. (1997) Biochemistry 36, 288–300.

[43] Segrest, J.P., Jones, M.K., Klon, A.E., Sheldahl, C.J., Hellinger, M., De Loof, H. and Harvey, S.C. (1999) J. Biol. Chem. 274, 31755–31758.

[44] Sparks, D.L., Phillips, M.C. and Lund-Katz, C. (1992) J. Biol. Chem. 267, 25830–25838.

[45] Calabresi, L., Meng, Q.H., Castro, G.R. and Marcel, Y.L. (1993) Biochemistry 32, 6477–6484.

[46] Bergeron, J., Frank, P.G., Scales, D., Meng, Q.H., Castro, G. and Marcel, Y.L. (1995) J. Biol. Chem. 270, 27429–27438.